Soft Matter

COMMUNICATION

View Article Online
View Journal | View Issue

Cite this: *Soft Matter*, 2026, **22**, 297

Received 17th August 2025,
Accepted 15th December 2025

DOI: 10.1039/d5sm00840a

rsc.li/soft-matter-journal

Probing the limits of effective temperature consistency in actively driven systems

Dima Boriskovsky, [a] Rémi Goerlich, [b] Benjamin Lindner [cd] and Yael Roichman *[ab]

We investigate the thermodynamic properties of a single inertial probe driven into a nonequilibrium steady state by random collisions with self-propelled active walkers. The probe and walkers are confined within a gravitational harmonic potential. We evaluate the robustness of the effective temperature concept in this active system by comparing values of distinct, independently motivated definitions: a generalized fluctuation–dissipation relation, a kinetic temperature, and *via* a work fluctuation relation. Our experiments reveal that, under specific conditions, these independent measurements coincide over a wide range of system configurations, yielding a remarkably consistent effective temperature. Furthermore, we also identify regimes where this consistency breaks down, which delineates the fundamental limits of extending equilibrium-like thermodynamic concepts to athermal, actively driven systems.

I. Introduction

A single colloidal particle confined within a harmonic potential and immersed in a thermal fluid offers a fundamental realization of a microscopic statistical thermometer.[1,2] In thermal equilibrium, the particle's random displacements follow a Boltzmann (Gaussian) distribution, allowing the thermodynamic temperature, T, of the surrounding environment to be directly determined by its mean potential energy *via* the principle of equipartition.[3]

Near and at equilibrium, T can be equivalently defined through various thermodynamic relations, which can be applied to and measured by a colloidal thermometer. Static relations, measured in stationary states, include canonical distributions and energy equipartition, as well as configurational definitions of temperature.[4,5] Dynamic relations, measured by probing the system's response properties, are given by the fluctuation–dissipation theorem,[6–10] which rigorously connects the effects of thermal noise and energy dissipation. In addition, fluctuation theorems also relate temperature to fluctuations in thermodynamic quantities such as heat, work, and entropy.[11–14]

Colloidal thermometers have thus been widely employed in experiments, both to validate theoretical measures of equilibrium temperature and to identify deviations from it.[15–18] Crucially, various definitions of absolute temperature must yield consistent, measurement-independent values in accordance with the zeroth law of thermodynamics.

In stark contrast, no universal definition for temperature exists for many natural and engineered systems that operate far from thermal equilibrium. Nonetheless, the notion of effective temperature has frequently arisen as a heuristic extension of equilibrium statistical mechanics to diverse systems operating far from equilibrium, including glassy materials,[19–23] biological suspensions,[15,16,24–28] driven granular media,[29–43] and active matter.[18,44–58]

In particular, under well-separated timescales, an equilibrium-like fluctuation–dissipation relation (FDR) can become applicable, leading to a definition of an effective temperature, T_{eff}. While the FDR-based T_{eff} has proven useful in various fields of physics,[17,59–62] its thermodynamic interpretation and range of applicability remain subjects of ongoing research.[63–67]

A remaining key challenge lies in identifying under which conditions distinct theoretical definitions of effective temperatures yield mutually consistent values far from equilibrium.[68,69] Further examples of nonequilibrium definitions that capture meaningful physical behavior in their statistical formulation include equipartition-based approaches, such as granular temperatures,[29,30] and those derived from fluctuation-relations (FR), applicable to both long-time nonequilibrium steady states (NESS) and nonequilibrium transitions.[12,38,70] Such definitions typically require stable steady states, the coexistence of stochastic and deterministic dynamics, and access to distinct NESS observables – conditions that are often difficult to achieve experimentally. Although no theoretical principle ensures the

[a] *Raymond & Beverly Sackler School of Physics and Astronomy, Tel Aviv University, Tel Aviv 6997801, Israel. E-mail: roichman@tauex.tau.ac.il*
[b] *Raymond & Beverly Sackler School of Chemistry, Tel Aviv University, Tel Aviv 6997801, Israel*
[c] *Bernstein Center for Computational Neuroscience Berlin, Philippstr. 13, Haus 2, 10115 Berlin, Germany*
[d] *Physics Department of Humboldt University Berlin, Newtonstr. 15, 12489 Berlin, Germany*

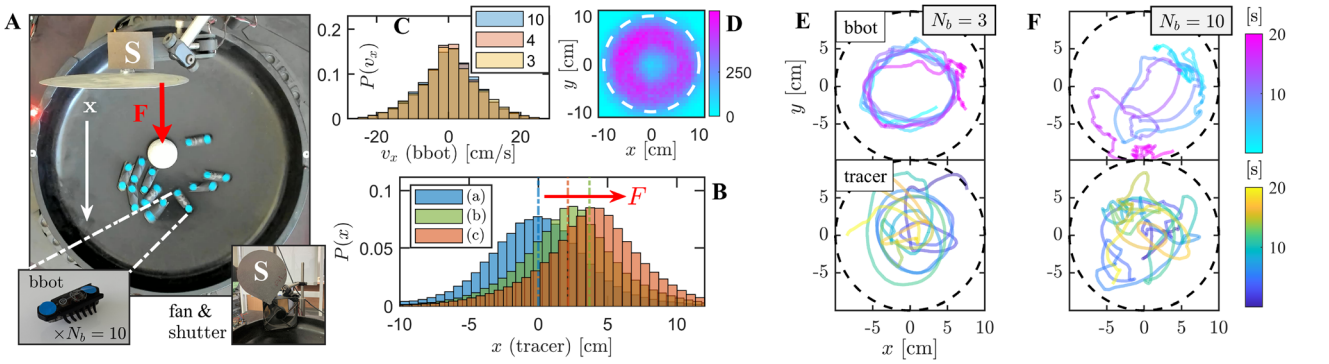

Fig. 1 The system: (A) experimental setup: a Styrofoam ball (diameter ∼4 cm, 1 g) is trapped in a gravitational harmonic potential, a plastic bowl (diameter 38 cm, depth 5 cm), and subjected to collisions with N_b = 10 self-propelled bbots (inset: standard bbot, 4 × 1 cm, 7.1 g). The ball is repeatedly perturbed with a uniform air stream created by an external fan along the x-axis (white arrow) to test a fluctuation-response relation. To enforce an abrupt onset and release of the perturbation, a mechanical shutter is used (denoted by 'S'). (B) Exemplary results (with N_b = 10) for three independent tracer's steady states: (a) an unperturbed state; (b) a weakly perturbed state (10 V fan operating voltage, $F_0 = \kappa\Delta x_\varepsilon \approx 62$ μN); and (c) a strongly perturbed state (13.5 V, $F_0 \approx 107.8$ μN). These stationary position distributions were obtained from combined time and ensemble averages, using 375 trajectories of 1 minute length. (C) Velocity distributions of bbot assemblies with different N_b = 3, 4, and 10. Instantaneous velocities were extracted from recordings of bbot trajectories tracked over 40 minutes using a frame rate of 30 frames per second (fps). (D) Spatial distribution of 10 bbots within the harmonic trap, with a soft boundary (steep curvature) indicated by a dashed circle of radius 10 cm. (E), (F) Typical 20 second trajectories of a single bbot in systems with N_b = 3 (E) and N_b = 10 (F) (upper panels), alongside the corresponding tracer trajectories (lower panels).

coincidence of these definitions far from equilibrium, our experiments indicate a range of conditions in which a consistent effective temperature can emerge in NESS, driven by active or athermal fluctuations (*cf.*[16,20,42]).

In this work, a statistical thermometer is realized experimentally, based on a macroscopic tracer particle confined in a harmonic trap and driven into a NESS by random inelastic collisions with self-propelled walkers (see Section 2 and Fig. 1). Previously,[71] it was shown that, with a large enough number of walkers, this system satisfies a linear (dynamic) FDR. Here, we assess the consistency of the FDR-based T_{eff} by comparing it to three independent measures: the tracer's potential energy and modified kinetic energy (in an unperturbed NESS), and a temperature based on a steady state work FR, in a NESS under a strong external perturbation. Our main result is displayed in Fig. 2: all three independent measurements of T_{eff} agree across a range of active bath parameters. We further compare our results with theoretical predictions and discuss conditions under which the consistency of T_{eff} breaks down.

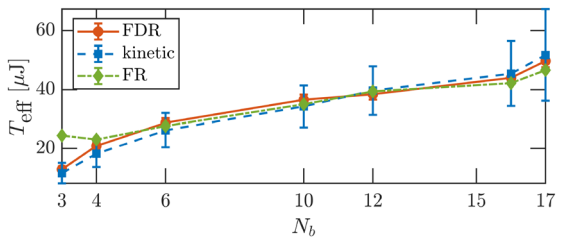

Fig. 2 Thermometer consistency: N_b = {3, 4, 6, 10, 12, 15, 17} bbots. Effective temperature measurements obtained using three independent methods: the potential temperature $T_{\text{pot}} = T_{\text{eff}}$ (circles, eqn (4)), the modified kinetic temperature $\tilde{T}_{\text{kin}}$ (squares, eqn (6)), and a constant temperature T_{FR} derived from a work FR (diamonds, eqn (7)). Notably, these static temperatures validate the FDR of eqn (2) (for $N_b > 3$) and define a consistent effective temperature T_{eff}.

II. Experimental setup and basic characterization

Our experimental setup is illustrated in Fig. 1(A): a lightweight styrofoam ball (the tracer) is confined within a parabolic plastic arena and is subjected to random collisions with an assembly of vibration-driven self-propelled particles (bristlebots, or bbots, specifically Hexbug™). The system is imaged from above using a standard webcam (Brio 4k, Logitech), and particle trajectories in the horizontal plane (XY) are extracted using a custom image analysis algorithm. The confining potential is approximately harmonic, with constant stiffness $\kappa = mga = 28.2 \pm 3$ g s^{-2}, set by the substrate curvature a, the gravitational acceleration g, and the tracer mass $m = 1 \pm 0.1$ g.

An external airflow can be applied *via* a fan (in the x direction) and abruptly switched-off by a physical shutter, affecting primarily the tracer particle. Stationary probability densities of the tracer's position along the x-axis for different intensities of air streams are shown in Fig. 1(B). The main effect of the air stream is a shift of the mean value of the histograms in the potential well, *i.e.*, an unperturbed state (a), a weakly perturbed state (b), and a strongly perturbed state (c). This mechanism is used to test the validity of both FDRs and FRs, as detailed in Sections 3.1 and 3.3 respectively (see SI, Fig. S1 and S2 for further details). We assume independent statistics along all axes and focus on analyzing the tracer's position and velocity components projected onto the x-axis, where the perturbation occurs.

A. Nonequilibrium properties of the active bath

In this setting, a single bbot with sufficient inertia typically performs circular motion around the trap center,[72] with a preferred chirality (clockwise for Hexbugs). As the number of bbots N_b increases, frequent collisions with other bbots (and the tracer) randomize their propulsion direction and result in

an active gas-like state (see SI, Movie S1). In particular, the bbot velocity distribution remains independent of N_b whereas its position distribution deviates from the original circular path with large N_b, as seen in Fig. 1(C) and (D).

Typical bbot trajectories are shown in Fig. 1(E) and (F). For N_b = 3, collisions are rare, and bbots follow long-lived circular paths; for N_b = 10, frequent collisions yield erratic, stochastic motion. In general, these self-propelled particles exhibit rich dynamics, including alignment with boundaries and emergent collective motion.[73] Here, the passive tracer primarily experiences random inelastic collisions with the active bbots (lower panels). These interactions introduce both noise and dissipation, which result in a collision-induced stochastic motion reaching a steady state within the harmonic potential. In this work, we focus on the properties of the tracer particle, as detailed below.

B. Nonequilibrium properties of the tracer

The NESS statistics and the dynamics of the tracer particle (in unperturbed conditions) are shown in Fig. 3, with the number of bbots N_b used as a control parameter. These results were obtained by averaging 375 particle trajectories of 1-minute duration and a time interval of Δt = 1/30 s.

Both the stationary position (x) and velocity (v_x) distributions of the tracer generally deviate from Gaussian behavior. As shown in Fig. 3(A), the position distribution evolves with increasing N_b, transitioning from an exponential form toward a Gaussian-like profile, particularly within the harmonic trap boundary $|x| < 10$ cm (for $|x| > 10$ cm the arena possesses a steeper curvature, *i.e.*, soft boundary for the trapped tracer and bbots). The velocity distributions (Fig. 3(B)) exhibit an exponential decay for small N_b = 3, with reliable statistics within $|v_x| < 50$ cm s^{-1}. At larger N_b, the velocity distributions converge to a distinct non-Gaussian shape that is well described by a stretched exponential function.

The stationary dynamics of the tracer are further characterized in Fig. 3(C) and (D) *via* the position and velocity autocorrelation functions (ACF). An increase in the rate of dissipative collisions upon adding more bbots, leads to more strongly damped tracer motion. This is reflected in a suppression of oscillations in the relaxation dynamics, and in the reduction of the relaxation time.

The position and velocity ACFs are well fit by the generic solution of a noisy damped harmonic oscillator (Fig. 3(E)). We focus on the velocity ACF that is given by,[2,74]

$$\bar{C}_{vv}(t) = \frac{C_{vv}(t)}{\langle v_x^2 \rangle_0} = e^{-\frac{t\gamma}{2}}\left(\cos \omega t - \frac{\gamma \sin \omega t}{2\omega}\right), \qquad (1)$$

where the bar indicates normalization, $\langle v_x^2 \rangle_0$ is the (stationary) velocity variance, with the angular brackets representing an ensemble average, and $\omega^2 \equiv \Omega^2 - \gamma^2/4$.

Fitting the ACF to eqn (1) provides system-specific values of the effective inverse timescales: the damping rate, γ, and the harmonic frequency, Ω. These inverse timescales are displayed in Fig. 3(F) as a function of N_b, showing a transition between underdamped ($\Omega < \gamma/2$) towards critically-damped ($\Omega \approx \gamma/2$) dynamics as N_b increases. A reduction in the relaxation time, $2\gamma^{-1}$, corresponds to an increase in collision frequency, evaluated by image analysis as the frequency of tracer-bbot collisions, τ_c^{-1} (black line).

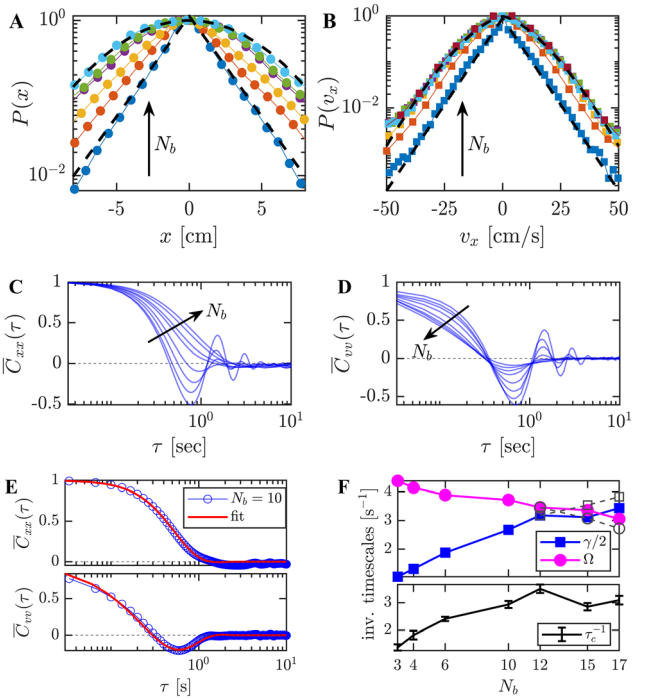

Fig. 3 NESS dynamics and statistics: data were obtained for active bath configurations with N_b = {3, 4, 6, 10, 12, 15, 17} bbots, using a tracer of mass m = 1 ± 0.1 g confined in a potential of stiffness κ = 28.2 ± 3 g s^{-2}. Results are obtained from combined time and ensemble averages over an ensemble of 375 one-minute-long tracer trajectories recorded at 30 fps for each N_b. (A) Rescaled position (x) distributions. Dashed line show fits to exponential (N_b = 3) and Gaussian (N_b = 15) functions. (B) Rescaled velocity (v_x) distributions. An exponential fit is shown for N_b = 3 and a stretched exponential fit for N_b = 15. (C), (D) Position (C) and velocity (D) autocorrelation functions (ACFs), showing increasingly damped dynamics with higher N_b. (E) Position and velocity ACFs for N_b = 10, fitted with eqn (1) using γ and Ω as fitting parameters, yielding consistent descriptions for both C_{xx} and C_{vv}. (F) Extracted relaxation rate (γ) and trapping frequency (Ω) as functions of N_b (upper panel). The impact of under-sampling on the observed dynamics is pronounced for large N_b (15 and 17). Hollow markers (dashed lines) show measurements at 30 fps, while colored markers correspond to 60 fps. The lower frame rate leads to apparent overdamped behavior, whereas the higher frame rate reveals dynamics consistent with a critically-damped regime. The collision frequency (τ_c^{-1}) is plotted *versus* N_b (lower panel), where τ_c is the measured mean-free time between tracer-bbot collisions.

At high densities (N_b = 15 and 17), fast sequential collisions require a higher temporal resolution to capture the tracer's inertial dynamics. In these cases, we perform and use additional recordings with Δt = 1/60 s to extract the effective inverse timescales (solid lines). At this sampling rate the fit parameters are consistent with the critical regime, whereas Δt = 1/30 s results in overdamped behavior (dashed lines). These measurements of velocity fluctuations and their corresponding system-specific inverse timescales are further discussed in the context of the kinetic temperature in Section 3.2.

III. Effective temperatures

In the following sections, we aim to assess whether three independent definitions of effective temperatures can yield mutually consistent values across different conditions and observables. Specifically, we examine the FDR for position and velocity observables under a step-perturbation (3.1), effective equipartition between kinetic and potential energies (3.2), and a work FR in a perturbed NESS (3.3).

A. FDR temperature

By subjecting the tracer to a small step-perturbation (an abrupt arrest of a constant force F_0 at $t = 0$), a linear FDR can be expressed for both position and velocity observables as[74,75] (setting $k_B = 1$):

$$R_x(t) = \frac{F_0}{T_{\text{eff}}} C_{xx}(t), \tag{2}$$

$$R_v(t) = \frac{F_0}{T_{\text{eff}}} C_{vx}(t), \tag{3}$$

where R_x and R_v are the mean response functions of the position and velocity observables, respectively. The correlation functions in the (long-time) unperturbed NESS are given by a position ACF, $C_{xx} = \langle x(t)x(0)\rangle_0$, and a position-velocity cross-correlation function, $C_{vx} = \langle v_x(t)x(0)\rangle_0$. In this context, an effective temperature T_{eff} is defined as a proportionality constant.

Notably, a static FDR can be recovered in eqn (2) at $t = 0$, with $C_{xx}(0) \to \langle x^2\rangle_0$ and $R_x(0) \to \Delta x_\varepsilon$, where $\langle x^2\rangle_0$ is the position variance in the unperturbed NESS, and $\Delta x_\varepsilon = \langle x\rangle_\varepsilon - \langle x\rangle_0$ is the mean displacement between the average position in the two steady states, perturbed (sub-index ε) and unperturbed (sub-index 0). Considering that $F_0 = \kappa \Delta x_\varepsilon$, the effective temperature T_{eff} coincides with the definition of potential energy equipartition,

$$T_{\text{pot}} = \kappa \langle x^2\rangle_0. \tag{4}$$

Thus, $T_{\text{eff}} = T_{\text{pot}}$ is always fulfilled when the system obeys the dynamic FDR in eqn (2), even in the presence of non-Gaussian steady state distributions.

Fig. 4(A) illustrates the experimental protocol designed to measure the system's linear response (see also ref. 71,76). The tracer is subjected to a small mechanical perturbation (external fan, 10 V operating voltage, $F_0 \approx 62$ μN on average). During an experiment, every two minutes, the fan is turned on for a minute and abruptly turned off at $t_0 = 60$ s for the following minute. In Fig. 4(B) we show the time-dependent ensemble averages $\langle x(t)\rangle$ and $\langle v_x(t)\rangle$, obtained with $N_b = 10$. These trajectories capture the relaxation dynamics towards a steady state following the force removal (a), as well as a perturbed steady state (b), characterized by a shifted mean Δx_ε (see also Fig. 1(B)).

Fig. 4(C) presents the corresponding FDR tests for both position and velocity observables. The system's full response to the abrupt force arrest at time $t_1 = t - t_0$ is evaluated as $R_x(t_1) = \langle x(t_1)\rangle - \langle x\rangle_0$ and $R_v(t_1) = \langle v_x(t_1)\rangle - \langle v_x\rangle_0$, and compared with the unperturbed correlation functions, C_{xx} and C_{xv}. Within measurement error, these results validate the FDRs given in eqn (2) and (3), with

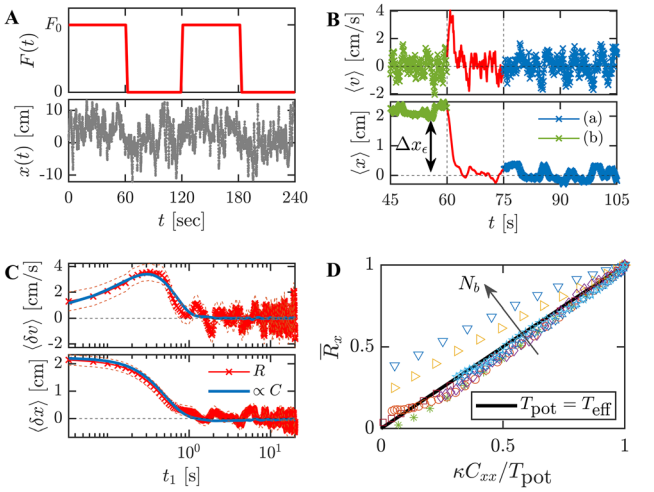

Fig. 4 FDR test of the full-response to a step-perturbation: results for mean values are obtained from pure ensemble averages over 375 two-minute step-perturbation sequences (at $t_0 = 60$ s), under weak external airflow applied by a fan at an operating voltage 10 V; correlation functions are computed in the steady state by a combined time and ensemble average. (A) Example of a typical perturbation sequence $x(t)$, where the fan is turned on for one minute and abruptly turned off for the subsequent minute. (B) Time-dependent mean velocity $\langle v_x(t)\rangle$ and mean position $\langle x(t)\rangle$. The shown interval captures the transient response following perturbation arrest (red line) and the unperturbed steady state (a), from which correlation functions are computed. The perturbed steady state is displaced from the trap center by $\Delta x_\varepsilon = 2.2$ cm (b). (C) FDR analysis using eqn (2) (lower panel) and eqn (3) (upper panel). These results were obtained with $N_b = 10$. (D) Parametric plot of position FDRs for $N_b = \{2, 3, 4, 6, 10, 12, 15, 17\}$ realizations, where the effective temperature T_{eff} determines the linear slope. In equilibrium-like behavior, all FDR data collapse onto a single line with slope $T_{\text{eff}} \sim \kappa\langle x^2\rangle_0$. Clear deviations from this equality are observed for the lowest densities ($N_b = 2$ and 3, triangles), indicating FDR violations.

an effective temperature determined by eqn (4). Thereby, in this system the tracer's potential temperature satisfies a dynamic FDR in both position and velocity observables. We note that the signal-to-noise ratio in R_v diminishes with increasing N_b, rendering the velocity response experimentally inaccessible for larger values ($N_b > 10$). The individual FDR tests of the experimental setups are further provided in the SI (see Fig. S4 and S5 therein).

Fig. 4(D) presents a parametric plot of the position FDR, showing normalized fluctuation and response quantities across different N_b configurations. Specifically, the solid linear line represents validation of eqn (2) with $T_{\text{eff}} = T_{\text{pot}}$. Violations of eqn (2) are mainly observed with the lowest $N_b = 2$ and 3, indicating a breakdown of the effective temperature description (as detailed in ref. 71). In contrast, with larger N_b, the tracer's potential temperature T_{pot} satisfies a dynamic FDR and is therefore consistent with T_{eff}.

B. Kinetic and potential energy partition

To probe deviations from equilibrium behavior, we define the tracer's kinetic temperature as,

$$T_{\text{kin}} = m\langle v_x^2\rangle_0. \tag{5}$$

As seen in Fig. 5, this definition seems to result in a contradiction between the kinetic and potential temperatures,

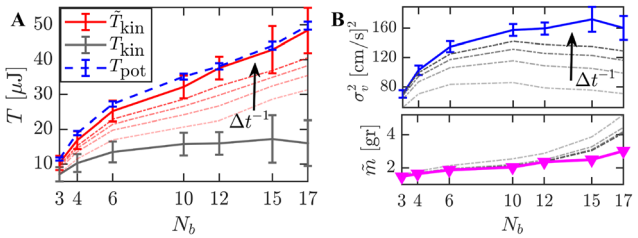

Fig. 5 The modified kinetic temperature: data are presented for configurations with N_b = {3, 4, 6, 10, 12, 15, 17} bbots, averaged over 375 one-minute tracer trajectories recorded in unperturbed conditions. (A) Comparison of the standard kinetic temperature T_{kin} (solid gray line), calculated using the tracer mass $m \approx 1$ g (eqn (5)), the modified kinetic temperature $\tilde{T}_{kin}$ (solid red line), evaluated using eqn (6), and the potential temperature T_{pot} (dashed blue line). Error bars indicate standard deviations. Dot-dashed red lines show deviations in $\tilde{T}_{kin}$ arising from increasing the measurement time interval Δt. (B) Separate contributions to $\tilde{T}_{kin}$: (upper panel) the velocity variance $\sigma_v = \langle v_x^2 \rangle_0$, and (lower panel) the effective mass $\tilde{m}$, evaluated from stationary ACF dynamics using eqn (1) and (6). Gray dot-dashed lines indicate deviations due to increasing Δt in both panels.

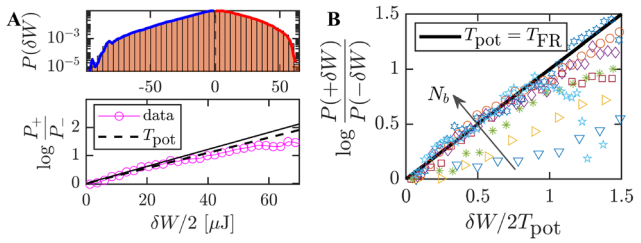

Fig. 6 Steady state work FR test: results present averages over 375 one-minute perturbed tracer trajectories, under a strong external airflow applied by a fan at an operating voltage 13.5 V. (A) Work FR test for N_b = 10. The upper panel shows an asymmetric work (δW) distribution in a NESS under a strong continuous perturbation (airflow). The temperature measurement of T_{FR}, extracted from a fit to eqn (7) (small δW, solid line), is consistent with the potential temperature (T_{pot}, dashed line) determined from the unperturbed definition in eqn (4). (B) Normalized plot of work FR tests across various N_b = {2, 3, 4, 6, 10, 12, 15, 17} configurations. The solid (black) line indicates an ideal agreement between the effective temperatures obtained from the work FR and from the equipartition definition ($T_{pot} = T_{FR}$), demonstrating thermodynamic-like consistency.

since deviations from the potential temperature T_{pot} (eqn (4)) are observed for all N_b configurations (solid gray line in Fig. 5(A)). Namely, T_{kin} saturates and becomes largely independent of N_b in the high-density limit. This clear mismatch is further supported by direct measurements of the effective trapping frequencies Ω, extracted from the tracer's velocity ACFs (see Fig. 3(F)). Across all system setups, Ω yields values lower than the natural frequency $\kappa/m \approx 5.3$ s^{-1}, even in an underdamped dynamic regime.

We note, however, that for tracer particles embedded in active or driven granular media, an effective mass emerges as a consequence of persistent athermal fluctuations and memory effects.[77–79] Accordingly, we define an effective mass, $\tilde{m} = \kappa\Omega^{-2}$, derived from the velocity correlations. Mapping the dynamics onto a linear Langevin equation, consistent with the ACF solution in eqn (1), relies on short persistence times and typically necessitates a modification of system parameters.[80,81] Consequently, the definition of the kinetic temperature is modified to,

$$\tilde{T}_{kin} = \tilde{m}\langle v_x^2 \rangle_0, \quad (6)$$

where $\tilde{m}$ is defined as a N_b-specific effective mass, under a constant potential stiffness κ. Using the effective mass to compute the kinetic temperature yields agreement between the two effective temperatures (solid red line in Fig. 5(A)). We note that the effective mass correction is derived from the correlation function of the unperturbed NESS, independent of both the step-response measurement and the FDR result (previous section).

Deviations of $\tilde{T}_{kin}$ measurements resulting from low measurement rates are shown as red dashed lines in Fig. 5(A). Fig. 5(B) shows the separate contributions to $\tilde{T}_{kin}$: the velocity variance $\langle v_x^2 \rangle_0$ (upper panel) and the effective mass $\tilde{m}$ (lower panel), across different N_b. We note that $\tilde{m}$ deviates from the tracer's actual mass (m = 1 g) and results in values that monotonically increase with N_b. Both measurements show a dependence on the sampling rate (Δt^{-1}), particularly for large $N_b > 10$ systems where $\langle v_x^2 \rangle_0$ saturates. Nevertheless, under well-resolved velocity fluctuations, the associated modified kinetic temperature $\tilde{T}_{kin}$ is consistent with the potential temperature T_{pot}, linking tracer dynamics with its linear response through $T_{eff} = T_{pot}$.

C. Effective temperature based on work FR

Here we investigate a work FR in a NESS subjected to a constant force $F_0 = \kappa\Delta x_\varepsilon$ (applied at time $t \to -\infty$). An asymmetric work distribution is obtained by the energetic fluctuation around the steady state, defined as $\delta W(t) = F_0\,[x_\varepsilon(t) - \langle x_\varepsilon \rangle]$. A steady state work FR can then be expressed as,[14,82,83]

$$\log \frac{P_\varepsilon(+\delta W)}{P_\varepsilon(-\delta W)} = \frac{\delta W}{2T_{FR}}, \quad (7)$$

where $P_\varepsilon(\pm\delta W)$ are negative and positive stationary work distributions, and T_{FR} is defined as an FR-based effective temperature.

Fig. 6(A) presents a work FR test conducted with N_b = 10. The upper panel shows the work distribution in a strongly perturbed steady state (state (c) in Fig. 1(B)). The red and blue lines correspond to positive and negative work fluctuations, respectively. In the lower panel, the left-hand side of eqn (7) is plotted as a function of δW. For small enough values of $\delta W < 80$ μJ, the probabilities are sufficiently sampled, and T_{FR} can be extracted from the slope of the linear relation (solid line). For large δW, deviations from linearity stem from limited sampling of these rare fluctuations.

The dashed linear line represents $T_{FR} = T_{pot}$, where T_{pot} is obtained independently in the unperturbed state (a). Namely, the two temperature measures agree, providing an experimental validation of the work FR (eqn (7)). This result can be extended to different N_b, as shown in Fig. 6(B). Here, the solid linear line represents $T_{FR} = T_{pot}$. Deviations for large values of the work fluctuations are expected due to under-sampling. Clear violations of eqn (7) are mainly observed for N_b = 2–4. For larger N_b systems, T_{FR} is also consistent with the FDR-based measure T_{eff}. Notably, these temperatures were measured in independent measurements under different perturbations.

This result shows that, for a broad range of parameters (N_b = 6–17), the same effective temperature that governs static (equipartition) and dynamic (FDR) properties of the system also rules the irreversibility of energy exchanges.

IV. Limitations of a consistent effective temperature

To further assess the range of consistency of effective temperature measures, we repeated the experiments from Section 3 for other system configurations. The standard experimental setup (detailed in Fig. 1 and shown in Fig. 7(A)) was modified by varying both the passive tracer and the surrounding active particles. Specifically, these modifications included: using a smaller styrofoam tracer particle (Fig. 7(B)); employing faster active bbots (Fig. 7(C)); and introducing a heavy tracer particle (Fig. 7(D)), *i.e.*, heavier than the bbots (m_{bot} = 7.1 g). Further system details are provided in the SI (see Fig. S6 and S8 therein).

Fig. 7(E) and (F) compare the tracer's modified kinetic temperature ($\tilde{T}_{kin}$) and potential temperature (T_{pot}) as a function of the number of bbots (N_b) for these configurations. The solid linear line represents the condition: $\tilde{T}_{kin} = T_{pot}$. In the alternative experimental setups that include a light tracer (Fig. 7(B) and (C)), $\tilde{T}_{kin}$ and T_{pot} coincide within measurement error and increase with N_b, consistent with our previous findings (Fig. 5). These systems can also yield consistent T_{eff} measurements whether *via* FDR (eqn 2) or work FR (eqn 7) tests (see details in SI). However, when replacing the lightweight tracers with a heavy tracer, we observe differences between the measured T_{pot} and $\tilde{T}_{kin}$ (see Fig. 7(F)).

Ultra-high-speed videos (SI, Movie S2) reveal the mechanical origin of this deviation. For lightweight tracers, interactions with the self-propelled bbots occur as discrete impacts, yielding a measurable ballistic regime between collisions. In contrast, heavy tracers can experience rapid recurrent collisions with the bbots, occurring on timescales shorter than the experimental sampling interval (Δt). Upon strong collisions the tracer visibly changes the bbot propulsion dynamics. In addition, the heavy tracer remains embedded among the bbots, whereas a lighter tracer may be kicked upwards, escaping entrapment.

These effects modify the coupling between tracer and environment and may thus lead to the observed discrepancy. We note that the external air-driven perturbation is generally too weak to induce a significant perturbation to the heavy tracer. Due to both effects, the FDR and FR tests fail for all considered N_b systems.

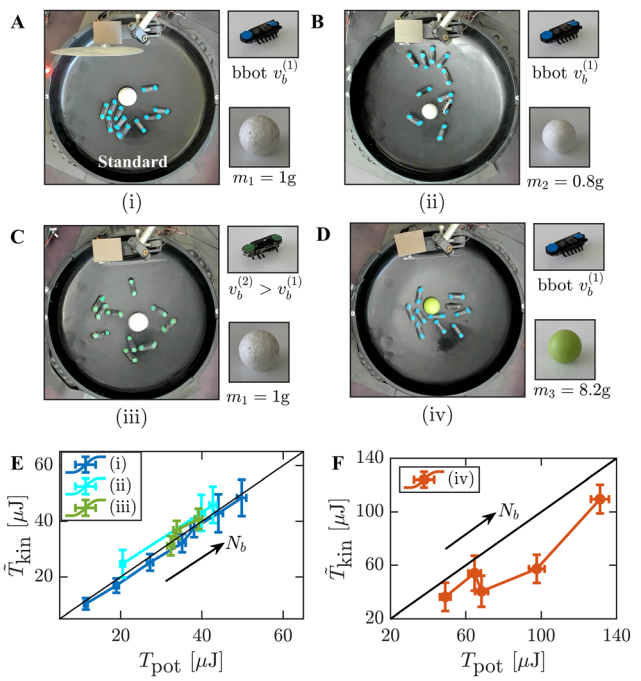

Fig. 7 Experimental applicability of effective temperature consistency. (A) Standard experimental setup as presented in Fig. 1 and detailed in Sections 2 and 3. (B) Configuration using a smaller Styrofoam tracer particle (m = 0.8 g, diameter 3.5 cm). (C) Configuration with faster self-propelled bbots (see SI for details). (D) Configuration employing a heavy tracer particle (m = 8.2 g, diameter 3.8 cm). (E) Comparison of energy partitioning between the modified kinetic temperature $\tilde{T}_{kin}$ (eqn (6)) and potential temperature T_{pot} (eqn (4)) as functions of N_b for configurations (i), (ii), and (iii). (F) Systematic violations of effective equipartition observed for configuration (D) with the heavy tracer, indicating the breakdown of thermodynamic-like consistency in this regime.

V. Summary and discussion

In this work, we have experimentally demonstrated that a passive granular tracer, confined in a harmonic potential and driven by an active fluctuating medium, can sustain a NESS that is well-characterized by a single effective temperature T_{eff}. This effective temperature serves as a unifying parameter that encapsulates both the system's dynamic response properties and its stationary fluctuations (as detailed in Fig. 2). We find that introducing an effective mass is essential to properly define the tracer's kinetic temperature, ensuring its consistency with the effective temperature of the NESS.

We identify three key features that appear essential to this equilibrium-like behavior of effective temperature consistency. First, both the spontaneous fluctuations of the tracer and its response to weak external perturbations are governed by the same physical mechanism, *i.e.* random collisions with the active medium.[71] This is manifested in the validity of a linear FDR.[10,62] Second, the light tracer is only weakly coupled to the environment, which minimizes the chance of physical entrapment or caging by bath particles, an effect known to induce long-term memory in the tracer's dynamics.[84,85] Finally, the bath dynamics (bbot motion) and the fluctuations they induce are largely unaffected by the external driving (airflow) that acts mainly on the tracer particle.[41,65,69]

The agreement between different definitions of effective temperatures observed here is unexpected for two reasons. First, the noise is a result of non-exponential collision times with the bath particles that show temporal correlation due to active self-propulsion. Under these conditions, the system exhibits non-trivial

steady state distributions, in variance with the Poisson shot noise conditions leading to Boltzmann-like steady states under which such agreement has been predicted.[28,86,87] Second, the use of an inertial tracer introduces memory effects in active matter, often breaking Markovian dynamics and precluding a single consistent effective temperature.[69,85,88,89] That this agreement persists despite these deviations from the idealized theoretical framework suggests a broader robustness of effective temperature concepts than previously recognized.

Conflicts of interest

There are no conflicts to declare.

Data availability

The data that support the findings of this study are available from the corresponding author, Y. R., upon reasonable request.

Supplementary information (SI) including supporting measurements and two movies is available. See DOI: https://doi.org/10.1039/d5sm00840a.

Acknowledgements

DB, RG and YR acknowledge support from the European Research Council (ERC) under the European Union's Horizon 2020 research and innovation program (grant agreement no. 101002392). BL would like to thank Deutsche Forschungsgemeinschaft for their support (DFG grant LI 1046/10-1).

References

1 G. E. Uhlenbeck and L. S. Ornstein, On the theory of the brownian motion, *Phys. Rev.*, 1930, **36**, 823.
2 M. C. Wang and G. E. Uhlenbeck, On the theory of the brownian motion ii, *Rev. Mod. Phys.*, 1945, **17**, 323.
3 H. Risken, *Fokker-planck equation*, Springer, 1996.
4 Y. Han and D. G. Grier, Configurational temperature of charge-stabilized colloidal monolayers, *Phys. Rev. Lett.*, 2004, **92**, 148301.
5 H. H. Rugh, Dynamical approach to temperature, *Phys. Rev. Lett.*, 1997, **78**, 772.
6 A. Einstein, On the motion of small particles suspended in liquids at rest required by the molecular-kinetic theory of heat, *Ann. Phys.*, 1905, **17**, 208.
7 P. Langevin, On the theory of brownian motion, *C. R. Acad. Sci.*, 1908, **146**, 530.
8 H. B. Callen and T. A. Welton, Irreversibility and generalized noise, *Phys. Rev.*, 1951, **83**, 34.
9 R. Kubo, The fluctuation-dissipation theorem, *Rep. Prog. Phys.*, 1966, **29**, 255.
10 R. Kubo, Brownian motion and nonequilibrium statistical mechanics, *Science*, 1986, **233**, 330.
11 G. Gallavotti and E. G. D. Cohen, Dynamical ensembles in nonequilibrium statistical mechanics, *Phys. Rev. Lett.*, 1995, **74**, 2694.
12 G. Gallavotti and E. Cohen, Nonequilibrium stationary states and entropy, *Phys. Rev. E: Stat., Nonlinear, Soft Matter Phys.*, 2004, **69**, 035104.
13 P. Jop, A. Petrosyan and S. Ciliberto, Work and dissipation fluctuations near the stochastic resonance of a colloidal particle, *Europhys. Lett.*, 2008, **81**, 50005.
14 J. R. Gomez-Solano, L. Bellon, A. Petrosyan and S. Ciliberto, Steady-state fluctuation relations for systems driven by an external random force, *Europhys. Lett.*, 2010, **89**, 60003.
15 K. C. Leptos, J. S. Guasto, J. P. Gollub, A. I. Pesci and R. E. Goldstein, Dynamics of enhanced tracer diffusion in suspensions of swimming eukaryotic microorganisms, *Phys. Rev. Lett.*, 2009, **103**, 198103.
16 C. Maggi, M. Paoluzzi, N. Pellicciotta, A. Lepore, L. Angelani and R. Di Leonardo, Generalized energy equipartition in harmonic oscillators driven by active baths, *Phys. Rev. Lett.*, 2014, **113**, 238303.
17 S. Ciliberto, Experiments in stochastic thermodynamics: Short history and perspectives, *Phys. Rev. X*, 2017, **7**, 021051.
18 R. Goerlich, L. B. Pires, G. Manfredi, P.-A. Hervieux and C. Genet, Harvesting information to control nonequilibrium states of active matter, *Phys. Rev. E*, 2022, **106**, 054617.
19 L. F. Cugliandolo, D. S. Dean and J. Kurchan, Fluctuation-dissipation theorems and entropy production in relaxational systems, *Phys. Rev. Lett.*, 1997, **79**, 2168.
20 I. K. Ono, C. S. O'Hern, D. J. Durian, S. A. Langer, A. J. Liu and S. R. Nagel, Effective temperatures of a driven system near jamming, *Phys. Rev. Lett.*, 2002, **89**, 095703.
21 L. Berthier and J.-L. Barrat, Shearing a glassy material: Numerical tests of nonequilibrium mode-coupling approaches and experimental proposals, *Phys. Rev. Lett.*, 2002, **89**, 095702.
22 S. Joubaud, B. Percier, A. Petrosyan and S. Ciliberto, Aging and effective temperatures near a critical point, *Phys. Rev. Lett.*, 2009, **102**, 130601.
23 E. Bouchbinder and J. Langer, Linear response theory for hard and soft glassy materials, *Phys. Rev. Lett.*, 2011, **106**, 148301.
24 X.-L. Wu and A. Libchaber, Particle diffusion in a quasi-two-dimensional bacterial bath, *Phys. Rev. Lett.*, 2000, **84**, 3017.
25 A. Argun, A.-R. Moradi, E. Pinçe, G. B. Bagci, A. Imparato and G. Volpe, Non-boltzmann stationary distributions and nonequilibrium relations in active baths, *Phys. Rev. E*, 2016, **94**, 062150.
26 C. Maggi, M. Paoluzzi, L. Angelani and R. Di Leonardo, Memory-less response and violation of the fluctuation-dissipation theorem in colloids suspended in an active bath, *Sci. Rep.*, 2017, **7**, 17588.
27 R. Wiese, K. Kroy and V. Holubec, Modeling the efficiency and effective temperature of bacterial heat engines, *Phys. Rev. E*, 2024, **110**, 064608.
28 C. Di Bello, R. Majumdar, R. Marathe, R. Metzler and É. Roldán, Brownian particle in a poisson-shot-noise active bath: exact statistics, effective temperature, and inference, *Ann. Phys.*, 2024, **536**, 2300427.
29 A. Puglisi, V. Loreto, U. M. B. Marconi and A. Vulpiani, Kinetic approach to granular gases, *Phys. Rev. E: Stat., Nonlinear, Soft Matter Phys.*, 1999, **59**, 5582.

30 T. Pöschel and S. Luding, *Granular gases*, Springer Science & Business Media, 2001.
31 J. Van Zon and F. MacKintosh, Velocity distributions in dissipative granular gases, *Phys. Rev. Lett.*, 2004, **93**, 038001.
32 R. Ojha, P.-A. Lemieux, P. Dixon, A. Liu and D. Durian, Statistical mechanics of a gas-fluidized particle, *Nature*, 2004, **427**, 521.
33 D. Villamaina, A. Puglisi and A. Vulpiani, The fluctuation-dissipation relation in sub-diffusive systems: the case of granular single-file diffusion, *J. Stat. Mech.*, 2008, **2008**, L10001.
34 D. Villamaina, A. Baldassarri, A. Puglisi and A. Vulpiani, The fluctuation-dissipation relation: how does one compare correlation functions and responses?, *J. Stat. Mech.*, 2009, **2009**, P07024.
35 Y. Shokef and D. Levine, Energy distribution and effective temperatures in a driven dissipative model, *Phys. Rev. E: Stat., Nonlinear, Soft Matter Phys.*, 2006, **74**, 051111.
36 G. Bunin, Y. Shokef and D. Levine, Frequency-dependent fluctuation-dissipation relations in granular gases, *Phys. Rev. E: Stat., Nonlinear, Soft Matter Phys.*, 2008, **77**, 051301.
37 A. Puglisi, A. Baldassarri and V. Loreto, Fluctuation-dissipation relations in driven granular gases, *Phys. Rev. E: Stat., Nonlinear, Soft Matter Phys.*, 2002, **66**, 061305.
38 K. Feitosa and N. Menon, Fluidized granular medium as an instance of the fluctuation theorem, *Phys. Rev. Lett.*, 2004, **92**, 164301.
39 A. R. Abate and D. J. Durian, Effective temperatures and activated dynamics for a two-dimensional air-driven granular system on two approaches to jamming, *Phys. Rev. Lett.*, 2008, **101**, 245701.
40 S. Joubaud, D. Lohse and D. Van Der Meer, Fluctuation theorems for an asymmetric rotor in a granular gas, *Phys. Rev. Lett.*, 2012, **108**, 210604.
41 A. Gnoli, A. Puglisi, A. Sarracino and A. Vulpiani, Nonequilibrium brownian motion beyond the effective temperature, *PLoS One*, 2014, **9**, e93720.
42 J.-Y. Chastaing, J.-C. Géminard and A. Naert, Two methods to measure granular gas temperature, *J. Stat. Mech.*, 2017, **2017**, 073212.
43 Z. Zeng, S. Zhang, X. Zheng, C. Xia, W. Kob, Y. Yuan and Y. Wang, Equivalence of fluctuation-dissipation and edwards' temperature in cyclically sheared granular systems, *Phys. Rev. Lett.*, 2022, **129**, 228004.
44 J. Palacci, C. Cottin-Bizonne, C. Ybert and L. Bocquet, Sedimentation and effective temperature of active colloidal suspensions, *Phys. Rev. Lett.*, 2010, **105**, 088304.
45 I. A. Martinez, E. Roldán, J. M. Parrondo and D. Petrov, Effective heating to several thousand kelvins of an optically trapped sphere in a liquid, *Phys. Rev. E: Stat., Nonlinear, Soft Matter Phys.*, 2013, **87**, 032159.
46 D. Levis and L. Berthier, From single-particle to collective effective temperatures in an active fluid of self-propelled particles, *Europhys. Lett.*, 2015, **111**, 60006.
47 E. Dieterich, J. Camunas-Soler, M. Ribezzi-Crivellari, U. Seifert and F. Ritort, Single-molecule measurement of the effective temperature in non-equilibrium steady states, *Nat. Phys.*, 2015, **11**, 971.
48 F. Ginot, I. Theurkauff, D. Levis, C. Ybert, L. Bocquet, L. Berthier and C. Cottin-Bizonne, Nonequilibrium equation of state in suspensions of active colloids, *Phys. Rev. X*, 2015, **5**, 011004.
49 I. Petrelli, L. F. Cugliandolo, G. Gonnella and A. Suma, Effective temperatures in inhomogeneous passive and active bidimensional Brownian particle systems, *Phys. Rev. E*, 2020, **102**, 012609.
50 E. Flenner and G. Szamel, Active matter: Quantifying the departure from equilibrium, *Phys. Rev. E*, 2020, **102**, 022607.
51 É. Fodor, C. Nardini, M. E. Cates, J. Tailleur, P. Visco and F. Van Wijland, How far from equilibrium is active matter?, *Phys. Rev. Lett.*, 2016, **117**, 038103.
52 M. Han, J. Yan, S. Granick and E. Luijten, Effective temperature concept evaluated in an active colloid mixture, *Proc. Natl. Acad. Sci. U. S. A.*, 2017, **114**, 7513.
53 A. Solon and J. M. Horowitz, On the einstein relation between mobility and diffusion coefficient in an active bath, *J. Phys. A*, 2022, **55**, 184002.
54 S. Ye, P. Liu, F. Ye, K. Chen and M. Yang, Active noise experienced by a passive particle trapped in an active bath, *Soft Matter*, 2020, **16**, 4655.
55 J. T. Park, G. Paneru, C. Kwon, S. Granick and H. K. Pak, Rapid-prototyping a Brownian particle in an active bath, *Soft Matter*, 2020, **16**, 8122.
56 J. F. Boudet, J. Jagielka, T. Guerin, T. Barois, F. Pistolesi and H. Kellay, Effective temperature and dissipation of a gas of active particles probed by the vibrations of a flexible membrane, *Phys. Rev. Res.*, 2022, **4**, L042006.
57 J. Shea, G. Jung and F. Schmid, Passive probe particle in an active bath: can we tell it is out of equilibrium?, *Soft Matter*, 2022, **18**, 6965.
58 G. Geva, T. Admon, M. Levin and Y. Roichman, Diffusive contact between randomly driven colloidal suspensions, *Phys. Rev. Lett.*, 2025, **134**, 218201.
59 U. M. B. Marconi, A. Puglisi, L. Rondoni and A. Vulpiani, Fluctuation-dissipation: response theory in statistical physics, *Phys. Rep.*, 2008, **461**, 111.
60 M. Baiesi, C. Maes and B. Wynants, Fluctuations and response of nonequilibrium states, *Phys. Rev. Lett.*, 2009, **103**, 010602.
61 C. Maes, Response theory: a trajectory-based approach, *Front. Phys.*, 2020, **8**, 229.
62 M. Baldovin, L. Caprini, A. Puglisi, A. Sarracino and A. Vulpiani, *The many faces of fluctuation-dissipation relations out of equilibrium*, Springer, 2022, pp. 29–57.
63 K. Martens, E. Bertin and M. Droz, Dependence of the fluctuation-dissipation temperature on the choice of observable, *Phys. Rev. Lett.*, 2009, **103**, 260602.
64 L. F. Cugliandolo, The effective temperature, *J. Phys. A: Math. Theor.*, 2011, **44**, 483001.
65 A. Puglisi, A. Sarracino and A. Vulpiani, Temperature in and out of equilibrium: A review of concepts, tools and attempts, *Phys. Rep.*, 2017, **709**, 1.
66 V. Holubec and R. Marathe, Underdamped active brownian heat engine, *Phys. Rev. E*, 2020, **102**, 060101.

67 B. Sorkin, H. Diamant, G. Ariel and T. Markovich, Second law of thermodynamics without einstein relation, *Phys. Rev. Lett.*, 2024, **133**, 267101.
68 J. Casas-Vázquez and D. Jou, Temperature in non-equilibrium states: a review of open problems and current proposals, *Rep. Prog. Phys.*, 2003, **66**, 1937.
69 L. Hecht, L. Caprini, H. Löwen and B. Liebchen, How to define temperature in active systems?, *J. Chem. Phys.*, 2024, **161**, 1.
70 A. Puglisi, P. Visco, A. Barrat, E. Trizac and F. van Wijland, Fluctuations of internal energy flow in a vibrated granular gas, *Phys. Rev. Lett.*, 2005, **95**, 110202.
71 D. Boriskovsky, B. Lindner and Y. Roichman, The fluctuation-dissipation relation holds for a macroscopic tracer in an active bath, *Soft Matter*, 2024, **20**, 8017.
72 O. Dauchot and V. Démery, Dynamics of a self-propelled particle in a harmonic trap, *Phys. Rev. Lett.*, 2019, **122**, 068002.
73 L. Giomi, N. Hawley-Weld and L. Mahadevan, Swarming, swirling and stasis in sequestered bristle-bots, *Proc. R. Soc. London, Ser. A*, 2013, **469**, 20120637.
74 M. Yaghoubi, M. E. Foulaadvand, A. Bérut and J. Luczka, Energetics of a driven brownian harmonic oscillator, *J. Stat. Mech.: Theory Exp.*, 2017, **2017**, 113206.
75 T. Haga, Nonequilibrium langevin equation and effective temperature for particle interacting with spatially extended environment, *J. Stat. Phys.*, 2015, **159**, 713.
76 K. Engbring, D. Boriskovsky, Y. Roichman and B. Lindner, A nonlinear fluctuation-dissipation test for markovian systems, *Phys. Rev. X*, 2023, **13**, 021034.
77 C. Maes, Fluctuating motion in an active environment, *Phys. Rev. Lett.*, 2020, **125**, 208001.
78 A. Seguin and P. Gondret, Added-mass force in dry granular matter, *Phys. Rev. E*, 2022, **105**, 054903.
79 M. Giona, G. Procopio and C. Pezzotti, Fluid-particle interactions and fluctuation-dissipation relations iii–correlated fluctuations, regularity and added mass, *arXiv*, preprint, 2024, arXiv:2412.19170, DOI: 10.48550/arXiv:2412.19170.
80 M. Wiśniewski, J. Łuczka and J. Spiechowicz, Effective mass approach to memory in non-Markovian systems, *Phys. Rev. E*, 2024, **109**, 044116.
81 J. Shea, G. Jung and F. Schmid, Force renormalization for probes immersed in an active bath, *Soft Matter*, 2024, **20**, 1767.
82 G. Wang, E. M. Sevick, E. Mittag, D. J. Searles and D. J. Evans, Experimental demonstration of violations of the second law of thermodynamics for small systems and short time scales, *Phys. Rev. Lett.*, 2002, **89**, 050601.
83 O. Narayan and A. Dhar, Reexamination of experimental tests of the fluctuation theorem, *J. Phys. A: Math. Gen.*, 2003, **37**, 63.
84 L. Berthier and J. Kurchan, Non-equilibrium glass transitions in driven and active matter, *Nat. Phys.*, 2013, **9**, 310.
85 L. Caprini, A. Ldov, R. K. Gupta, H. Ellenberg, R. Wittmann, H. Löwen and C. Scholz, Emergent memory from tapping collisions in active granular matter, *Commun. Phys.*, 2024, **7**, 52.
86 B. Dybiec, E. Gudowska-Nowak and I. M. Sokolov, Underdamped stochastic harmonic oscillator driven by lévy noise, *Phys. Rev. E*, 2017, **96**, 042118.
87 K. Kanazawa, T. G. Sano, T. Sagawa and H. Hayakawa, Minimal model of stochastic athermal systems: Origin of non-Gaussian noise, *Phys. Rev. Lett.*, 2015, **114**, 090601.
88 L. Caprini, R. K. Gupta and H. Löwen, Role of rotational inertia for collective phenomena in active matter, *Phys. Chem. Chem. Phys.*, 2022, **24**, 24910.
89 A. R. Sprenger, L. Caprini and H. Lo,-wen, and R. Wittmann, Dynamics of active particles with translational and rotational inertia, *J. Phys.: Condens. Matter*, 2023, **35**, 305101.